2-1-2021

Effective inhibition of SARS-CoV-2 entry by heparin and enoxaparin derivatives

Ritesh Tandon
University of Mississippi Medical Center

Joshua S. Sharp
University of Mississippi

Fuming Zhang
Center for Biotechnology & Interdisciplinary Studies

Vitor H. Pomin
University of Mississippi

Nicole M. Ashpole
University of Mississippi

See next page for additional authors

Recommended Citation

Tandon, R., Sharp, J. S., Zhang, F., Pomin, V. H., Ashpole, N. M., Mitra, D., McCandless, M. G., Jin, W., Liu, H., Sharma, P., & Linhardt, R. J. (2021). Effective inhibition of sars-cov-2 entry by heparin and enoxaparin derivatives. Journal of Virology, 95(3), e01987-20. https://doi.org/10.1128/JVI.01987-20

AMERICAN SOCIETY FOR MICROBIOLOGY | Journal of Virology®

VACCINES AND ANTIVIRAL AGENTS

Effective Inhibition of SARS-CoV-2 Entry by Heparin and Enoxaparin Derivatives

Ritesh Tandon,[a] Joshua S. Sharp,[b,c] Fuming Zhang,[d] Vitor H. Pomin,[b] Nicole M. Ashpole,[b] Dipanwita Mitra,[a] Martin G. McCandless,[a] Weihua Jin,[d] Hao Liu,[b] Poonam Sharma,[a] Robert J. Linhardt[d]

[a]Department of Microbiology and Immunology, University of Mississippi Medical Center, Jackson, Mississippi, USA
[b]Department of BioMolecular Sciences, University of Mississippi, Oxford, Mississippi, USA
[c]Department of Chemistry and Biochemistry, University of Mississippi, Oxford, Mississippi, USA
[d]Center for Biotechnology and Interdisciplinary Studies, Rensselaer Polytechnic Institute, Troy, New York, USA

ABSTRACT Severe acute respiratory syndrome-related coronavirus 2 (SARS-CoV-2) has caused a pandemic of historic proportions and continues to spread globally, with enormous consequences to human health. Currently there is no vaccine, effective therapeutic, or prophylactic. As with other betacoronaviruses, attachment and entry of SARS-CoV-2 are mediated by the spike glycoprotein (SGP). In addition to its well-documented interaction with its receptor, human angiotensin-converting enzyme 2 (hACE2), SGP has been found to bind to glycosaminoglycans like heparan sulfate, which is found on the surface of virtually all mammalian cells. Here, we pseudotyped SARS-CoV-2 SGP on a third-generation lentiviral (pLV) vector and tested the impact of various sulfated polysaccharides on transduction efficiency in mammalian cells. The pLV vector pseudotyped SGP efficiently and produced high titers on HEK293T cells. Various sulfated polysaccharides potently neutralized pLV-S pseudotyped virus with clear structure-based differences in antiviral activity and affinity to SGP. Concentration-response curves showed that pLV-S particles were efficiently neutralized by a range of concentrations of unfractionated heparin (UFH), enoxaparin, 6-*O*-desulfated UFH, and 6-*O*-desulfated enoxaparin with 50% inhibitory concentrations (IC_{50}s) of 5.99 μg/liter, 1.08 mg/liter, 1.77 μg/liter, and 5.86 mg/liter, respectively. In summary, several sulfated polysaccharides show potent anti-SARS-CoV-2 activity and can be developed for prophylactic as well as therapeutic purposes.

IMPORTANCE The emergence of severe acute respiratory syndrome coronavirus (SARS-CoV-2) in Wuhan, China, in late 2019 and its subsequent spread to the rest of the world has created a pandemic situation unprecedented in modern history. While ACE2 has been identified as the viral receptor, cellular polysaccharides have also been implicated in virus entry. The SARS-CoV-2 spike glycoprotein (SGP) binds to glycosaminoglycans like heparan sulfate, which is found on the surface of virtually all mammalian cells. Here, we report structure-based differences in antiviral activity and affinity to SGP for several sulfated polysaccharides, including both well-characterized FDA-approved drugs and novel marine sulfated polysaccharides, which can be developed for prophylactic as well as therapeutic purposes.

KEYWORDS spike glycoprotein, COVID-19, coronavirus, glycosaminoglycan, heparan sulfate, pseudotyping

The recent emergence of severe acute respiratory syndrome coronavirus 2 (SARS-CoV-2) in Wuhan, China, in late 2019 and its subsequent spread to the rest of the world has created a pandemic situation unprecedented in modern history (1–4). SARS-CoV-2 is a betacoronavirus closely related to SARS-CoV; however, significant differences in the spike glycoprotein (SGP) are present in SARS-CoV-2 that may drive differences in

Citation Tandon R, Sharp JS, Zhang F, Pomin VH, Ashpole NM, Mitra D, McCandless MG, Jin W, Liu H, Sharma P, Linhardt RJ. 2021. Effective inhibition of SARS-CoV-2 entry by heparin and enoxaparin derivatives. J Virol 95:e01987-20. https://doi.org/10.1128/JVI.01987-20.

Editor Tom Gallagher, Loyola University Chicago

Address correspondence to Joshua S. Sharp, jsharp@olemiss.edu, or Robert J. Linhardt, linhar@rpi.edu.

Received 7 October 2020
Accepted 5 November 2020
Accepted manuscript posted online 10 November 2020
Published 13 January 2021

the attachment and entry process (5). In SARS-CoV-2, the SGP binds to its cognate receptor, human angiotensin-converting enzyme 2 (hACE2). The bound virus is then endocytosed, and SGP is acted upon in the cell by the endosomal protease TMPRSS2 to allow envelope fusion and viral entry (6).

While ACE2 has been confidently identified as the viral receptor, many viruses (including some betacoronaviruses) use cellular polysaccharides as cellular attachment coreceptors, allowing the virus to adhere to the surface of the cell and increasing the local concentration of viral particles to increase effective infection rates (7, 8). Sequence analysis of SGP of SARS-CoV-2 suggests that this virus has evolved to have additional potential glycosaminoglycan (GAG) binding domains compared to SARS-CoV (5, 9). GAGs are a family of linear sulfated polysaccharides found on the surface of virtually all mammalian cells and commonly include chondroitin sulfate (CS) and heparan sulfate (HS). The glycocalyx represents a thick layer on the surface of the epithelium to which the virus needs to adhere and which it needs to penetrate to reach its protein-based receptor (10). The HS GAGs, anchored to the cell membrane through their core proteins, are large, linear, anionic polysaccharide chains that extend away from the cell membrane, through the glycocalyx (composed of glycolipids and glycoproteins close to the cell surface), and form an anionic canopy above the cell (5). These HS GAG chains represent the first point of contact for many pathogens, including parasites, bacteria, and viruses (11). Pathogens such as SARS-CoV-2 exploit the natural function of HS-PGs in which the host cell's GAG chains capture HS-binding proteins (HS-BPs) (i.e., growth factors and chemokines) from the extracellular milieu, guiding them down the HS chains through the glycocalyx to their protein-based receptors, where they act as a coreceptor for cell signaling (7, 10). Previous studies using isolated SARS-CoV-2 SGP monomer or trimer and surface plasmon resonance (SPR) have shown that SARS-CoV-2 SGP has high affinity to unfractionated heparin (UFH) (5, 9), a specialized member of the HS family that is highly sulfated and commonly used clinically as an anticoagulant drug. It was also reported that UFH was capable of inhibiting infection of SARS-CoV-2 in Vero cell culture in a concentration-dependent fashion (9). These results support a model of SARS-CoV-2 attachment and entry where SARS-CoV-2 initially binds to HS in the nasal epithelium glycocalyx (possibly in the olfactory neuroepithelium, where the apical surface is rich in HS [12]), subsequently binds hACE2, and is endocytosed.

However, little work has been done in this area due in part to concerns about the safety of the assay. Due to the highly transmissible and pathogenic nature of SARS-CoV-2, handling of live virus requires biosafety level 3 (BSL-3) containment (13). Thus, only facilities equipped for BSL-3 can safely study neutralizing responses using live virus. There is a need for a safer way to study viral inhibitors and immunological responses in a practical, reproducible surrogate assay that effectively replaces the need for the live SARS-CoV-2, extending the capability of carrying out such studies to non-BSL-3 laboratories, which are more widely available. Here, we report the development and use of a high-titer lentivirus pseudotyped with SARS-CoV-2 SGP to screen potential inhibitors in a lower-biosafety-level laboratory. Since the backbone of this virus consists of a nonreplicating lentivirus, it poses no risk of infection to the personnel involved, and attachment and entry can be measured by detectable fluorescence intensity directly correlating with the efficiency of transduction. Using this lentiviral system, we tested the ability of various sulfated polysaccharides to inhibit pseudotyped viral attachment and entry. We found several sulfated polysaccharides with potent anti-SARS-CoV-2 activity. We demonstrate that SPR can be performed using pseudotyped lentiviral virions, presenting a more biologically relevant context for biophysical analysis than isolated SGP protein. We discuss implications of these findings for both SARS-CoV-2 studies and potential clinical applications. The low serum bioavailability of intranasally administered UFH (14–16), along with data suggesting that the nasal epithelium is a portal for initial infection and transmission (17–19), suggests that intranasal administration of UFH may be an effective and safe prophylactic treatment.

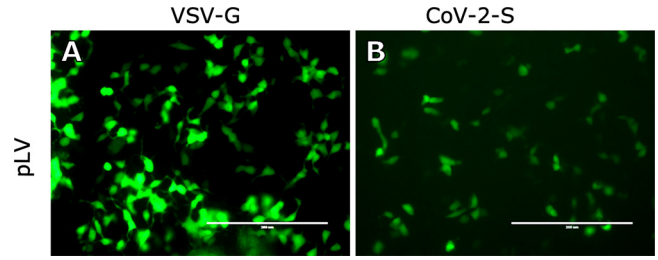

FIG 1 Transduction of HEK293T cells with lentiviral vector (pLV) pseudotyped with (A) VSV-G or (B) CoV-2-SGP. The lentiviral backbone incorporates enhanced green fluorescent protein (eGFP) that is expressed upon integration into target cells. The fluorescence was recorded at 48 h postransduction. Magnification, ×20. Bar, 200 μm.

RESULTS

SARS-CoV-2 spike protein can be efficiently pseudotyped on a lentiviral vector. We used a third-generation lentiviral vector (pLV) (20, 21) to pseudotype SARS-CoV-2 SGP for the purpose of these studies. Both vesicular stomatitis virus glycoprotein (VSV-G) and SARS-CoV-2 spike glycoprotein pseudotyped pLV efficiently, although VSV-G was much more efficient, as expected (Fig. 1). The success of pseudotyping was assessed by the expression of green fluorescent protein (GFP), since the pLV backbone incorporates the gene encoding GFP.

pLV-S transduction inhibited by some sulfated polysaccharides. We tested the ability of 12 different polysaccharides to inhibit pLV-S transduction in HEK293T cells to determine if SARS-CoV-2 attachment and entry can be inhibited by abrogating the interaction of SGP with cellular HS via the addition of exogenous sulfated polysaccharides. Results of a blinded analysis of GFP transduction results are shown in Fig. 2. Several polysaccharides exhibited a substantial, concentration-dependent inhibition of pLV-S transduction. Different polysaccharide structures exhibited vastly different inhibitory effects. Mammalian chondroitin sulfate and a mixture of GAGs isolated from silver-banded whiting (*Sillago argentifasciata*) consisting of 90% chondroitin sulfate and 10% hyaluronic acid (22) showed poor inhibitory qualities. Both UFH and enoxaparin (a low-molecular-weight heparin drug) had high apparent inhibitory activity in our screen, with UFH showing more activity, consistent with SPR affinity results (5). Interestingly, two marine sulfated glycans showed high inhibitory activity in our screen: sulfated fucan, isolated from *Lytechinus variegatus* (sea urchin), and sulfated galactan from *Botryocladia occidentalis* (red seaweed) (23). The structures of heparin, sulfated fucan, and sulfated galactan are shown in Fig. 3. None of these polysaccharides had a significant impact on cell viability in this assay (data not shown).

No clear structural consistencies in inhibitors were found; fucans and galactans have monosaccharide structures and linkages different from those of heparin, as well as different sulfation patterns. Overall, sulfate density is similar between sulfated fucan, sulfated galactan, and cell surface HS. We performed selective desulfation of both UFH and enoxaparin and screened them against our pLV-S system to probe structure-function relationships in sulfated polysaccharide SARS-CoV-2 inhibitory activity. Complete desulfation of both UFH (UFH-fully-deS) and enoxaparin (enoxaparin-fully-deS) greatly decreased anti-SARS-CoV-2 activity. Selective desulfation at the *N* position of GlnN (UFH-deNS and enoxaparin-deNS) similarly decreased inhibitory activity of both UFH and enoxaparin, consistent with previous SPR results (5, 9). In contrast with previous SPR results, however, we found that selective desulfation at the 6-*O* position of GlcN (UFH-de6S and enoxaparin-de6S) did not significantly reduce inhibitory activity of either UFH or enoxaparin. Proton nuclear magnetic resonance (NMR) analysis revealed the successful selective desulfation of these samples (Fig. 4), indicating that 6-*O*-sulfation is not required for anti-SARS-CoV-2 activity in a pseudotyped transduction model.

Anti-SARS-CoV-2 IC_{50} determination for heparin derivatives. To test the potency and efficacy of these sulfated glycans, we performed concentration-dependent pseudotype pLV-S infection assays to determine 50% inhibitory concentrations (IC_{50}s) for

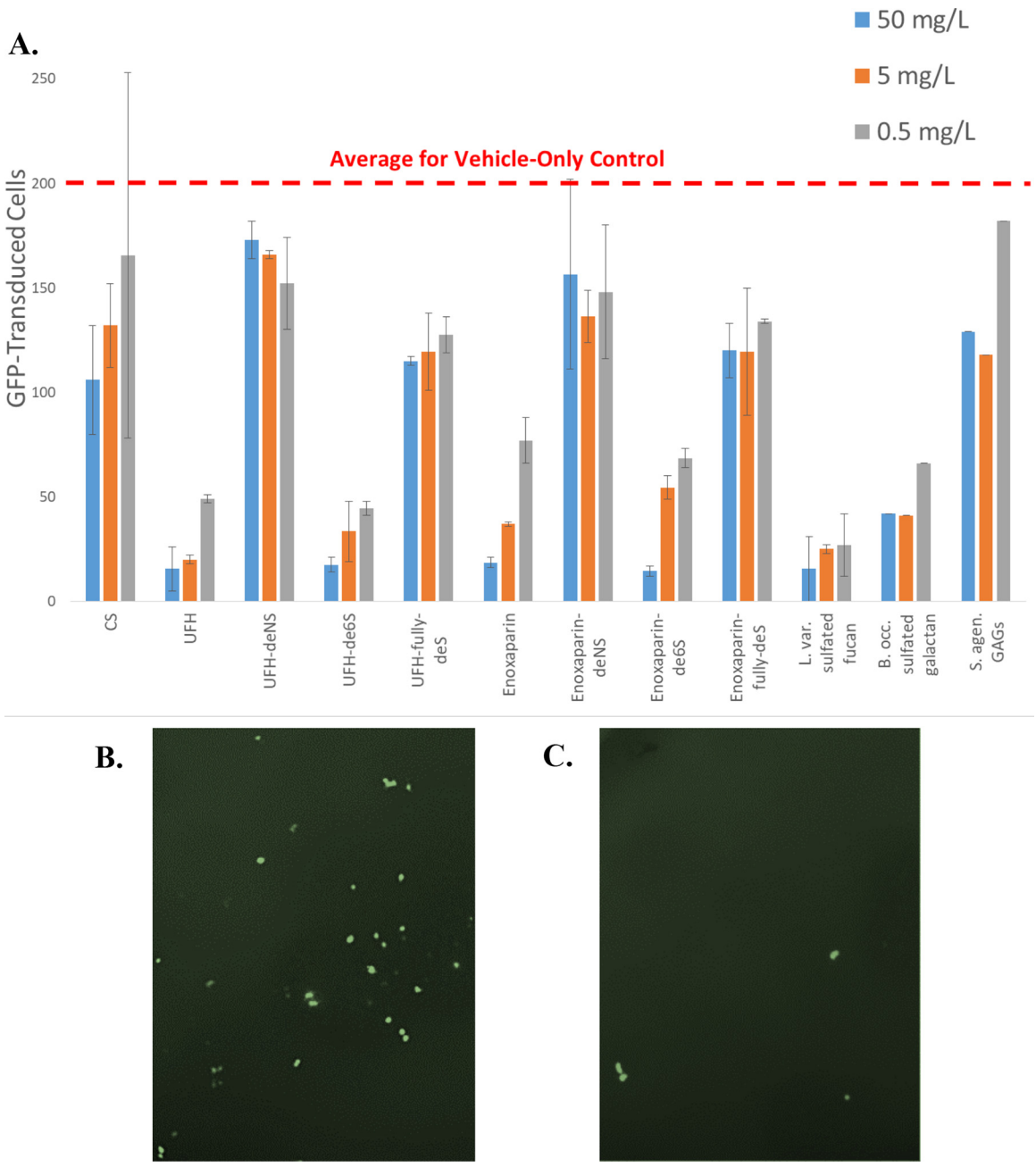

FIG 2 SARS-CoV-2 SGP pseudotyped lentiviral screen for inhibition of attachment and entry. (A) Quantitation of GFP-transduced cells in the presence of each inhibitor at three concentrations. Average GFP transduction of control was 200.2 cells per well. (B) Representative fluorescence microscopy of the UFH-deNS inhibitor assay. (C) Representative fluorescence microscopy of the UFH inhibitor assay.

UFH, UFH-de6S, enoxaparin, enoxaparin-de6S, enoxaparin-deNS, enoxaparin-fully-deS, *L. variegatus* SF, and *B. occidentalis* SG. Because of the role of avidity often found in protein-GAG interactions, IC_{50}s were measured in milligrams per liter. We tested pLV-S transduction rates at inhibitor concentrations ranging from 500 mg/liter to 5 μg/liter; results are shown in Fig. 5. Both UFH and UFH-de6S gave very low IC_{50}s: 5.99 μg/liter and 1.77 μg/liter, respectively. The IC_{50} of UFH of 5.99 μg/liter is equivalent to a concentration of ~400 pM, which is 10× higher than K_D (dissociation constant) measurements of UFH to SARS-CoV-2 SGP by SPR (5). IC_{50} curve fits of UFH and UFH-de6S have substantial uncertainty due to a lack of sufficient data at concentrations below 5 μg/liter; however, the trend is clear. Enoxaparin and enoxaparin-de6S have substantially

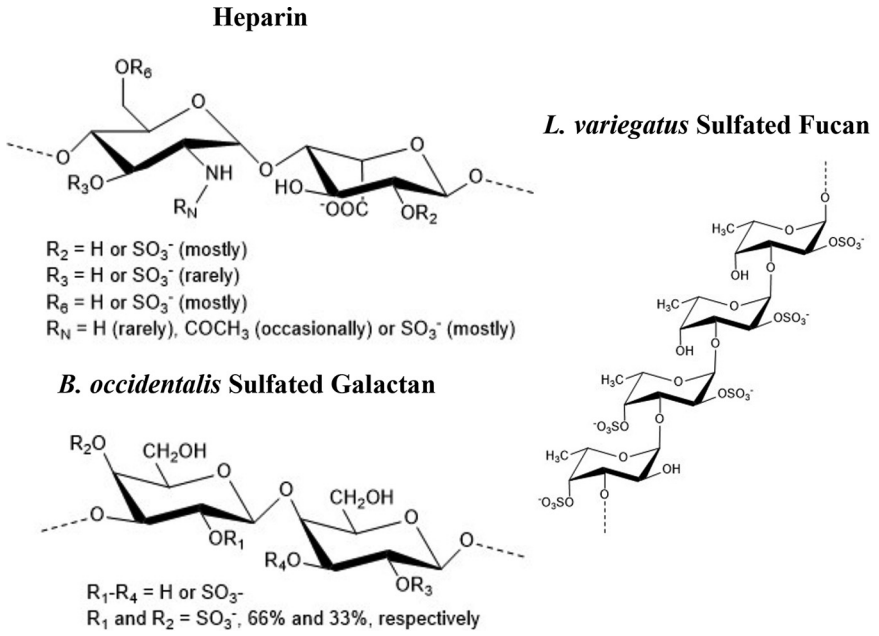

FIG 3 Structure of anti-SARS-CoV-2 sulfated polysaccharides. Enoxaparin and UFH differ primarily by the average length of the polysaccharide chain (average MW of UFH, ~15 kDa; average MW of enoxaparin, ~4.5 kDa). Enoxaparin-de6S and UFH-de6S have H at position R_6. Enoxaparin-deNS and UFH-deNS have H or Ac at R_N. Enoxoparin-fully-deS and UFH-fully-deS have no SO_3^- groups. The average MW of marine sulfated glycans is ≥100 kDa.

weaker inhibitory activities, with IC_{50}s of 1.08 mg/liter and 5.86 mg/liter, respectively. A separate batch of pLV-S was used to determine IC_{50}s for sulfated fucan, sulfated galactan, enoxaparin-deNS, and enoxaparin-fully-deS. Detailed IC_{50} results are summarized in Table 1.

SPR measurements of pLV-S binding affinity. Direct binding measurements of pLV-S for surface immobilized UFH were made ($n = 5$) at concentrations ranging from 0.08 nM to 1.4 nM (Fig. 6). Molar concentrations of the pLV-S virion were determined from an estimated molecular weight for pLV-S of 250 MDa. This molecular weight was based on the similarity of pLV to another enveloped retrovirus (Rous sarcoma virus) having a diameter of ~100 nm (24) and an estimated mass of 250 MDa (25). An on rate (k_a) of 2.9×10^6 M^{-1} s^{-1} ($\pm 1.1 \times 10^5$), an off-rate (k_d) of 2.4×10^{-3} s^{-1} ($\pm 1.9 \times 10^{-5}$), and a dissociation constant (K_D) of 8.5×10^{-10} M were determined in these direct binding measurements, which is comparable to the IC_{50} of UFH determined in Table 1.

A variety of oligosaccharides and polysaccharides at 1 μM were next examined for their ability to compete with immobilized UFH for pLV-S binding. Of the GAGs examined, only soluble heparins, heparan sulfate, dermatan sulfate, and chondroitin sulfates D and E were able to compete. Competitive binding was observed only for a very large heparin-derived octadecasaccharide (Fig. 6). The heparins showing binding in the competition experiments were examined at a range of concentrations to estimate their SPR-based IC_{50}s. Soluble UFH, nonanticoagulant heparin (TriS; heparin sulfated at R_N, R_2 and R_6 as shown in Fig. 3), and a nonanticoagulant low-molecular-weight heparin (NACH) showed IC_{50}s estimated by SPR of 125 nM, 500 nM, and 25 μM, respectively (data not shown).

DISCUSSION

Here, we report the development of a lentiviral pseudotyping system for SARS-CoV-2 and its use in screening potential viral entry inhibitors. While a few pseudotyping systems for SARS-CoV-2 are in development, this report provides evidence that lentiviral pseudotyped SARS-CoV-2 can be used to identify potential inhibitors for follow-up

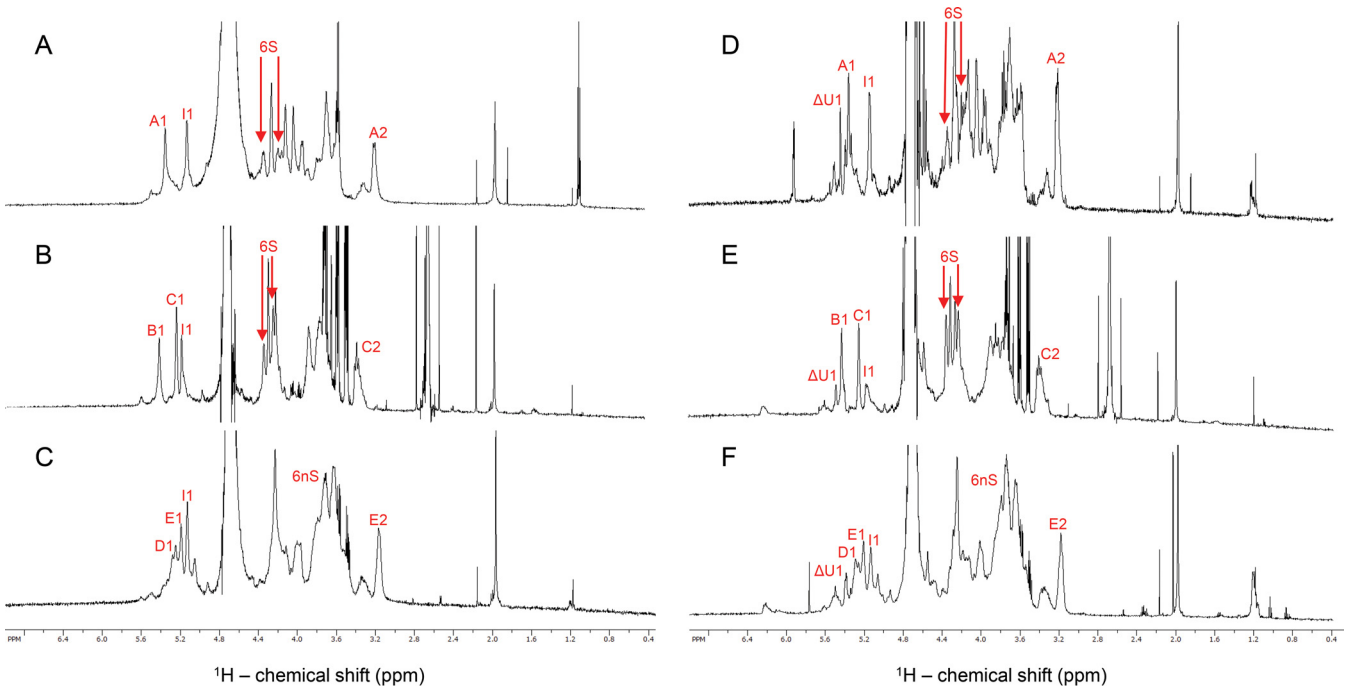

FIG 4 1D ^{1}H NMR spectra of (A) UFH, (B) UFH-deNS, (C) UFH-de6S, (D) LMWH, (E) LMWH-deNS, and (F) LMWH-de6S (expansion $\Delta\delta_H$, 7.0 to 0.4 ppm). The signals which were diagnostic for the desulfation reaction are labeled with letters and numerals according to the monosaccharide types, positions of the protons within the sugar rings, and 6-sulfation (6S) or non-6-sulfation (6nS). The letters A, B, C, D, E, and I denote, respectively, α-Glc*N*,6diS, α-Glc*N*Ac(6S), α-Glc*N*6S, α-Glc*N*Ac, α-Glc*N*S, and α-IdoA2S. The 6-sulfation in the α-Glc*N*Ac(6S) cannot be ensured solely on the basis of the anomeric assignment (signal B1).

studies in mouse models and clinical trials. These pseudoparticles can also be utilized for screening of inhibitors of SGP-hACE2 binding and resultant virus entry through biophysical methods such as SPR, with results that are arguably more biologically relevant than those obtained with isolated SGP. Their ability to both infect cells and respond to heparin in a manner consistent with previously published results from active SARS-CoV-2 (9) suggests that this lentiviral pseudotyping system may be useful for screening potential viral entry inhibitors, as they represent SGP on their surface in its native conformation.

The use of the pseudotyped systems to conveniently test potential inhibitors of viral attachment and entry has allowed us to perform structure-function analysis to begin to understand the important characteristics of inhibitory sulfated polysaccharides. Our finding that enoxaparin, a partially depolymerized heparin with an average molecular weight of ~4.5 kDa, has lower potency than UFH (average molecular weight,

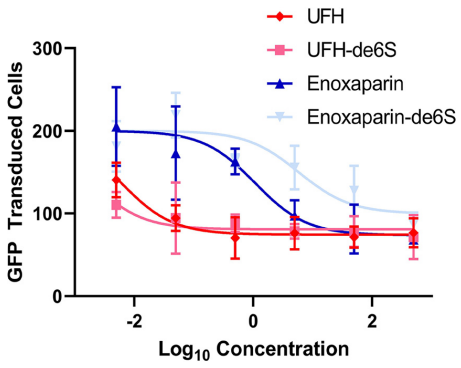

FIG 5 Relative IC_{50} curves for four potent SARS-CoV-2 inhibitors. Curves were modeled using GraphPad Prism 8.4.2. The top limit was set at the average vehicle-only control level for this assay batch (200.2), with the bottom limit allowed to float independently for each inhibitor. Details are shown in Table 1.

TABLE 1 Summary of IC_{50} calculations for SARS-CoV-2 inhibitors[a]

	IC_{50} (per liter)		Bottom limit (per cell)[b]	
Inhibitor	**Value**	**95% CI**	**Value**	**95% CI**
UFH	5.99 μg	2.90–11.96 μg	74.38†	64.28–84.36
UFH-de6S	1.77 μg	61.4–4,903 ng	80.76†	68.46–92.97
Enoxaparin	1.08 mg	247–4,164 μg	73.64†	45.44–99.54
Enoxaparin-de6S	5.86 mg	0.374–59.49 mg	99.71†	53.15–132.00
L. variegatus sulfated fucan	33.2 μg	15.5–68.7 μg	20.42‡	9.45–31.23
B. occidentalis sulfated galactan	54.0 μg	26.3–103.4 μg	24.75‡	15.43–33.95
Enoxaparin-deNS	No activity			
Enoxaparin-fully-deS	No activity			

[a]CI, confidence interval.
[b]†, assay batch with a vehicle-only average transduction of 200.2 cells; ‡, assay batch with a vehicle-only average transduction of 120.2 cells. Bottom limits are not directly comparable between batches.

~15 kDa) even in terms of milligrams per liter is consistent with previous SPR results (5), as well as SPR results presented here (Fig. 6). The lower potency and higher K_D of the partially depolymerized heparin are consistent with a binding interaction that involves multiple binding sites on each UFH polysaccharide molecule, which we have also found in some of our previous studies of protein-GAG interactions (26, 27). These results are also consistent with previous sequence analysis of the S protein of SARS-CoV-2, which suggests the possibility of multiple heparin binding sites (5), as well as experiments with the receptor binding domain of the S protein, which showed binding at ~40× lower affinity (7), possibly due to the lack of avidity from binding sites in other domains.

Our results here show that a pseudotyped lentivirus system binds very tightly to UFH and HS, indicating the possible use of HS as an adhesion coreceptor. Moreover, addition of UFH and certain other sulfated polysaccharides inhibits attachment and entry of the pLV-S system with very high potency, suggesting that the role of heparan sulfate binding in attachment and entry is important. Recent results from Clausen and coworkers (7) further showed that removal of cell surface HS prevented infection of cells by both VSV pseudotyped with the SARS-CoV-2 S protein and actual SARS-CoV-2 virus in multiple cell types. Clausen et al. similarly showed that SARS-CoV (which also uses the ACE2 receptor) is not as effectively blocked by removal of cell surface HS (7). This is consistent with previous reports showing the SARS-CoV-2 S protein bound UFH 1,000× more tightly than the SARS-CoV S protein (5). Taken together, these data suggest a model where SARS-CoV-2 uses cell surface HS as an adhesion coreceptor to facilitate attachment to the cell surface. Clausen et al. also reported that binding of UFH to S protein causes increased interaction with ACE2 (7), possibly due to a conformational change of the S protein upon UFH binding previously reported by Mycroft-West et al. (9). Together, our data support a model where SARS-CoV-2 attaches to cell surface HS in a polysaccharide structure-dependent manner. The attached SARS-CoV-2 then engages with the ACE2 receptor, potentially in a ternary complex.

As shown in Fig. 2, the inhibitory abilities of UFH, sulfated fucan and sulfated galactan from marine sources suggest that there is considerable flexibility in the SGP GAG binding site(s). UFH, sulfated fucan from *L. variegatus*, and sulfated galactan from *B. occidentalis* all demonstrate substantial inhibitory potency, even though they do not share monosaccharide composition, glycosidic linkage sites or stereochemistry, or sites of sulfation (Fig. 3). However, the poor inhibitory activity of chondroitin sulfate indicates that inhibition is not merely a question of presenting a negative charge on a linear polymer. The role of structural specificity rather than negative charge density is also supported by some of the SPR competition results presented here; dermatan sulfate, which largely has one sulfo group per disaccharide, competed for SGP binding similarly to CS-D and CS-E, which have two sulfo groups per disaccharide (Fig. 6B). Also

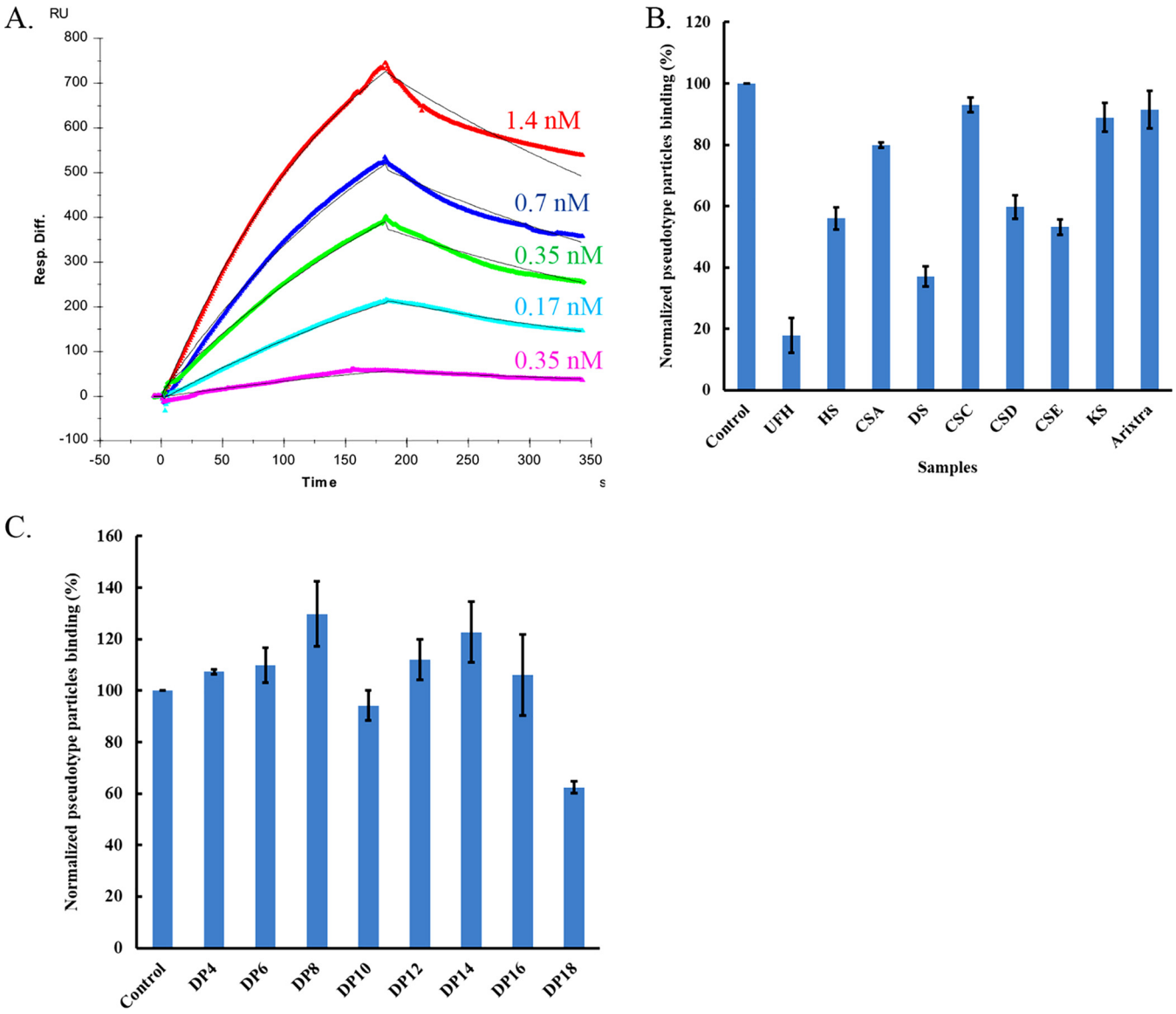

FIG 6 SPR measures affinity of pLV-S virion binding to various GAGs. (A) SPR sensorgrams of pLV-S binding to immobilized heparin. Virion concentration is based on an estimated molecular weight of 250 MDa. (B and C) Normalized pLV-S virion binding to surface-immobilized heparin upon competition with different GAGs in solution (B) or different-length heparin-derived oligosaccharides in solution (C). Pseudotype virions were present at 0.35 nM, and GAGs were present at 1,000 nM. All results represent triplicate measurements, with error bars representing one standard deviation.

supporting some degree of structural specificity of the SGP GAG binding site(s) are the results from specifically chemically desulfated UFH and enoxaparin. While complete desulfation and specific *N*-desulfation greatly decrease the potency of both UFH and enoxaparin to inhibit SARS-CoV-2 attachment and entry, 6-*O*-desulfation has little effect on potency and no effect on efficacy in this assay (Fig. 5 and Table 1). These results are similar but not identical to previously described SPR results for GAG binding to SGP monomers and trimers (5, 9). In this study, we undertook SPR studies on pLV-S to better understand the interaction of a pseudovirus particle containing multiple surface SGPs. The studies that rely entirely on the ectodomain or an excised receptor binding domain (RBD) may be missing important structural features induced by the enveloped virus context. The pLV-S showed very tight (~1 nM) binding to immobilized UFH that could be effectively competed with using soluble UFH and nonanticoagulant heparin. Further studies to characterize both pLV-S and SGP-sulfated polysaccharide interactions are required to understand the optimal binding structure(s).

Due to high morbidity and mortality rates, COVID-19 has captured the attention of scientists from a range of fields, and several vaccine candidates as well as therapies are in development (28, 29). The ability of various sulfated polysaccharides to inhibit SARS-CoV-2 attachment and entry with high potency presents intriguing and novel opportunities for therapeutic and prophylactic drug development. Of particular immediate interest are UFH and enoxaparin, two drugs widely used for anticoagulation therapy. However, both drugs have substantial side effects, including bleeding, Moreover, both drugs are currently being used as anticoagulants in some COVID-19 cases where evidence of microclotting, such as high D-dimer levels, is present (30). The systemic use of UFH or enoxaparin as a COVID-19 antiviral treatment or prophylactic has the potential for dangerous side effects and presents a risk of serious complications with potential anti-coagulation COVID-19 treatments. There remains considerable potential for non-systemic use of UFH or enoxaparin as antiviral treatment or prophylaxis. Previous results from both humans (15, 16) and rodents (14, 31) indicate that even very large doses of UFH and enoxaparin administered via inhalation result in very poor serum bioavailability. These results suggest that COVID-19 treatment via an intranasal or inhalation route should avoid dangerous side effects or complications with anticoagulation treatments while potentially still providing a prophylactic or therapeutic benefit. Recent published reports indicate that the nasal epithelium is a probable major portal for initial infection and transmission based on viral loads in both symptomatic and asymptomatic patients (18, 19), as well as expression patterns of both the hACE2 receptor and the TMPRSS2 protease (17). This suggests that a self-administered nasal spray of UFH may be a simple, safe, and effective prophylactic to lower the rates of SARS-CoV-2 transmission. While single intranasal administration of both UFH and enoxaparin in a rat model resulted in no noted toxicity and very poor serum bioavailability (14), we are aware of no studies of repeated dosing of UFH. Longer-term toxicology and pharmacokinetic studies of intranasal UFH, enoxaparin, and 6S derivatives of the two are under way.

MATERIALS AND METHODS

Materials. Enoxaparin sodium injection (Winthrop/Sanofi, Bridgewater, NJ, USA) was used as provided. Heparan sulfate sodium salt from bovine kidney, heparin sodium salt from porcine intestinal mucosa (molecular weight [MW], 18 kDa), *N*-methyl-*N*-(trimethylsilyl)trifluoroacetamide (MSTFA), and Dowex 50WX8-100 ion-exchange resin were purchased from Sigma-Aldrich Inc. (St. Louis, MO, USA). Chondroitin sulfate sodium salt was purchased from Santa Cruz Biotechnology, Inc. (Dallas, TX, USA). For SPR studies, Arixtra (M_w = 1,727 Da) was purchased from Pharmaceutical Buyers, Inc. (New Hyde Park, NY), porcine intestinal heparan sulfate (HS) (M_w = 14 kDa) was from Celsus Laboratories (Cincinnati, OH), chondroitin sulfate A (CS-A) (M_w = 20 kDa) from porcine rib cartilage was from Sigma (St. Louis, MO), dermatan sulfate (DS) (M_w = 30 kDa) from porcine intestine was from Sigma, chondroitin sulfate C (CS-C) (M_w = 20 kDa) from shark cartilage was from Sigma, chondroitin sulfate D (CS-D) (M_w = 20 kDa) from whale cartilage was from Seikagaku (Tokyo, Japan), and chondroitin sulfate E (CS-E) (M_w = 20 kDa) from squid cartilage was from Seikagaku. Keratan sulfate (KS) was prepared from bovine cornea as previously described (32). Nonanticoagulant low-molecular-weight HP (NACH) was synthesized from dalteparin, a nitrous acid depolymerization product of porcine intestinal HP, followed by periodate oxidation (33). Nonanticoagulant heparin TriS (NS2S6S) was synthesized from *N*-sulfo heparosan with subsequent modification with C5-epimerase and 2-*O*- and 6-*O*-sulfotransferases (2OST and 6OST1/6OST3) (34). Heparin oligosaccharides included tetrasaccharide, hexasaccharide, octasaccharide, decasaccharide, dodecasaccharide, tetradecasaccharide, hexadecasaccharide, and octadecasaccharide and were prepared from porcine intestinal UFH via controlled partial heparin lyase 1 treatment followed by size fractionation. Sensor SA chips were from GE Healthcare (Uppsala, Sweden). SPR measurements were performed on a Biacore 3000 system operated using Biacore 3000 control and BIAevaluation software (version 4.0.1).

Generation of pseudotype particles. HEK293T cells (ATCC number CRL3216) were cultured in Dulbecco modified Eagle medium (DMEM) (Corning Inc.) supplemented with 10% fetal bovine serum (FBS; Fisher Scientific) at 37°C with 5% CO_2. HEK293T cells (2×10^6) were plated in a 100-mm tissue culture dish and transfected the next day, when they were about 75% confluent, with a combination of the following plasmids: 9 μg of pLV-eGFP a gift from Pantelis Tsoulfas (Addgene [http://n2t.net/addgene:36083] plasmid number 36083; RRID Addgene_36083), 9 μg of psPAX2 (a gift from Didier Trono; Addgene plasmid number 12260; RRID Addgene_12260), and 3 μg of pCAGGS-S (SARS-CoV-2) (catalog no. NR-52310; BEI Resources) or VSV-G (a gift from Tannishtha Reya; Addgene plasmid number 14888; RRID Addgene_14888) as a control. Polyethylenimine (PEI) reagent (Millipore Sigma number 408727) was used for transfection following the manufacturer's protocols. The next day, the cells were checked for transfection efficiency under a fluorescence microscope, indicated by GFP

fluorescence. The supernatants from cell culture at 24 h were harvested and stored at 4°C, and more (10 ml) complete medium (DMEM containing 10% FBS) was added to the plates. The supernatant from cell culture at 48 h was harvested and combined with the 24-h supernatant for each sample. The combined supernatants were spun in a tabletop centrifuge for 5 min at 2,000 $\times$ *g* to pellet the residual cells and then passed through a 0.45-μm syringe filter. Aliquots were frozen at −80°C. New HEK293T cells plated in 12-well tissue culture dishes were infected with the harvested virus (supernatant) with a dilution range of 10^2 to 10^7. Virus (pLV-S) titers were calculated by counting the GFP-positive cells in the dilution with 20 to 100 GFP-positive cells.

Inhibitor screening. Serial dilutions of the potential inhibitors (500, 50, 5, 0.5, 0.05, and 0.005 mg/liter) were made in DMEM with end volumes of 50 μl each. Fifty microliters of the supernatant pLV-S stock (diluted to give 200 to 300 GFP-positive cells/well) was mixed with the diluted samples, incubated for 1 h at 37°C, then laid over HEK293T cells plated in 96-well tissue culture dishes, and incubated at 37°C and 5% CO_2 for 2 h. Medium was replaced with complete medium (DMEM containing 10% FBS) and incubated for another 48 h. Cells were fixed in 3.7% formaldehyde, and the assay was read on Lionheart FX automated fluorescence microscope (BioTek Instruments, Inc., Winooski, VT, USA). The total number of cells per well was counted using the Object Count feature in Nikon Elements AR Analysis version 5.02 by a blinded observer. Debris was gated using a restriction criterion of an area between 20 and 1,000 pixels. Data were analyzed in Prism 8 (GraphPad, Inc.). Relative IC_{50}s were calculated in Prism 8 using a fixed top limit of the average vehicle-only control level (200.2 for the first batch of inhibitors; 120.2 for the second batch) and a floating bottom limit. For the cell viability studies, polysaccharides were diluted in 100 μl of the raw cell culture medium (DMEM) to achieve a concentration of 0.05 g/liter, incubated for 1 h at 37°C, then laid over HEK293T cells plated in 24-well tissue culture dishes, and incubated at 37°C and 5% CO_2 for 2 h. Cell viability was recorded by trypan blue exclusion assay on an automated cell counter (Bio-Rad TC20). Triplicate samples were used, and standard errors of the means were plotted as error bars.

Heparin and enoxaparin sodium desulfation for pseudotyped virus inhibition. Prior to desulfation, UFH and enoxaparin sodium were first converted to their pyridinium salts by passing through a self-packed cation-exchange column with Dowex 50 W resin, followed by lyophilization (35). For *N*-desulfation, 1 mg pyridinium salts was resuspended in 1 ml 5% methanol in dimethyl sulfoxide (DMSO) and heated at 50°C for 1.5 h. The sample was diluted and purified with a 3-kDa Amicon Ultra centrifugal filter (Millipore, Temecula, CA, USA) to remove low-molecular-weight impurities (36). For 6-*O*-desulfation, 1 mg pyridinium salts was added to 10 volumes (wt/wt) of MSTFA and 100 volumes (vol/wt) of pyridine. The mixture was incubated at 100°C for 30 min and then quickly cooled in an ice bath (37). The sample was dried under nitrogen gas flow and purified with a 3-kDa Amicon Ultra centrifugal filter (Millipore, Temecula, CA, USA) to remove low-molecular-weight impurities. Selectively desulfated products were analyzed by proton NMR to determine the extent and specificity of desulfation as detailed below. For full desulfation, 1 mg pyridinium salts was resuspended in 1 ml 10% methanol in DMSO and heated at 100°C for 6 h (38). The fully desulfated products were dried and administered as pyridinium salts for further studies.

NMR analysis of selective desulfation. The four heparin derivatives were subjected to one-dimensional (1D) ^{1}H NMR analysis together with the unmodified standards to confirm the selective removal of sulfation at the *N* and 6-*O* positions of the α-Glc*N*,6diS units in UFH and low-molecular-weight heparin (LMWH) after the reactions. Figure 4 illustrates the resultant spectra in which characteristic peaks were assigned and labeled to straightforwardly recognize the structural integrity of each sample. As expected, the two peaks assigned as 6S belonging to the two protons in the C-6$H_2OSO_3^-$ site present δ_H at the downfield region close to 4.2 ppm (spectra in Fig. 4A, B, D, and E), while the peak labeled as 6nS with δ_H at the more upfield region between 3.6 ppm and 3.7 ppm (spectra in Fig. 4C and F) is typical of the non-6-sulfated site of the glucosamine unit. This confirms that the 6-*O*-desulfation reaction occurred successfully for samples UFH-de6S (Fig. 4C) and LMWH-de6S (Fig. 4F), respectively, and that this type of sulfation was maintained as original in all other heparin samples. As a consequence of the 6-O-desulfation, the anomeric ^{1}H signals of Glc*N*Ac (assigned as D) and Glc*NS* (assigned as E) became resolved in the spectra of the UFH-de6S and LMWH-de6S samples, while the major A1 peak of the Glc*N*,6diS clearly seen in the spectrum of the controls and the 2-*O*-desulfated versions disappeared. Note also that the A2 and E2 peaks with δ_H close to 3.2 ppm of the unmodified standard and 6-*O*-desulfated heparins are at the same place, indicative of *N*-sulfation. This indicates that the 6-*O*-desulfation reaction was very selective, acting only on the 6-*O*-sulfation sites, and did not cause any unexpected removal on the *N*-sulfation sites of the same glucosamine units in the heparin derivatives.

Similarly to the displacement of the NMR signals related to 6-*O*-sulfation, the 2-*O*-desulfation caused a shift solely of the A2 peaks (δ_H close to 3.2 ppm) from the original positions on the UFH and LMWH samples to the new upfield position of δ_H close to 3.3 ppm, as indicated by the labeled signal C2 in the UFH-deNS (Fig. 4B) and LMWH-deNS (Fig. 4E). This shift is indicative of stereospecific desulfation at the *N* position. The unchanged peaks labeled as 6S on these heparin versions clearly confirm that the 6-*O*-sulfation was preserved after the selective *N*-desulfation reaction. The peaks labeled as B1 and C1 belong to anomers of the glucosamine units which are unsulfated at the *N* position. Note that these peaks show distinct δ_H of the original A1 signals in the heparin standards and of the E1 signals of both the UFH-6deS and LMWH-6deS samples, which are all *N*-sulfated.

Surface plasmon resonance. Biotinylated UFH was prepared by conjugating its reducing end to amine-PEG3-Biotin (Pierce, Rockford, IL). In brief, UFH (2 mg) and amine-PEG3-biotin (2 mg; Pierce, Rockford, IL) were dissolved in 200 μl H_2O, and 10 mg $NaCNBH_3$ was added. The reaction mixture was heated at 70°C for 24 h; after that, a further 10 mg $NaCNBH_3$ was added and the reaction mixture was

heated at 70°C for another 24 h. After cooling to room temperature, the mixture was desalted with the spin column (molecular weight cutoff [MWCO], 3,000). Biotinylated UFH was collected, freeze-dried, and used for SA chip preparation. The biotinylated UFH was immobilized to streptavidin (SA) chips based on the manufacturer's protocol. The successful immobilization of UFH was confirmed by the observation of a 600-resonance-unit (RU) increase on the sensor chip. The control flow cell (FC1) was prepared by 2 min injection with saturated biotin.

Direct binding of the pseudotype particles to surface immobilized UFH was determined by SPR. The pseudotype particle samples were diluted in HBS-EP buffer (0.01 M HEPES, 0.15 M NaCl, 3 mM EDTA, 0.005% surfactant P20; pH 7.4). Different dilutions of pseudotype particle samples were injected at a flow rate of 30 μl/min. At the end of the sample injection, the same buffer flowed over the sensor surface to facilitate dissociation. After a 3-min dissociation time, the sensor surface was regenerated by injecting with 30 μl of 2 M NaCl to obtain a fully regenerated surface. The response was monitored as a function of time (sensorgram) at 25°C.

Solution competition studies on pseudotype particles, between UFH immobilized on the chip surface and soluble heparins, heparin-oligosaccharides, or other GAGs, were performed using SPR. Pseudotype particles (0.35 nM) mixed with 1 μM or various concentrations of heparins, heparin-derived oligosaccharides, or GAGs in HBS-EP buffer were injected over a UFH chip at a flow rate of 30 μl/min. After each run, the dissociation and the regeneration were performed as described above, and where binding was observed at 1 μM, the IC_{50} was determined.

ACKNOWLEDGMENTS

We acknowledge the receipt of pCAGGS-S plasmid from Florian Krammer at Icahn School of Medicine at Mount Sinai Hospital, NY. We also acknowledge William P. Vignovich, Francisco F. Bezerra, and Bernadeth F. Ticar for purifying and providing us with the *B. occidentalis* SG, *L. variegatus* SF, and *S. argentifasciata* GAGs, respectively.

Partial funding for this work was provided by the University of Mississippi Medical Center. H.L. and J.S.S. acknowledge funding from the National Institute of General Medical Sciences (R01GM127267). N.M.A. acknowledges funding from the National Institute of General Medical Sciences (P30GM122733). R.T. acknowledges funding from NASA (80NSSC19K1603).

REFERENCES

1. Zhu N, Zhang D, Wang W, Li X, Yang B, Song J, Zhao X, Huang B, Shi W, Lu R, Niu P, Zhan F, Ma X, Wang D, Xu W, Wu G, Gao GF, Tan W, China Novel Coronavirus Investigating and Research Team. 2020. A novel coronavirus from patients with pneumonia in China, 2019. N Engl J Med 382:727–733. https://doi.org/10.1056/NEJMoa2001017.
2. Wu F, Zhao S, Yu B, Chen YM, Wang W, Song ZG, Hu Y, Tao ZW, Tian JH, Pei YY, Yuan ML, Zhang YL, Dai FH, Liu Y, Wang QM, Zheng JJ, Xu L, Holmes EC, Zhang YZ. 2020. A new coronavirus associated with human respiratory disease in China. Nature 579:265–269. https://doi.org/10.1038/s41586-020-2008-3.
3. Perlman S. 2020. Another decade, another coronavirus. N Engl J Med 382:760–762. https://doi.org/10.1056/NEJMe2001126.
4. Gates B. 2020. Responding to Covid-19—a once-in-a-century pandemic? N Engl J Med 382:1677–1679. https://doi.org/10.1056/NEJMp2003762.
5. Kim SY, Jin W, Sood A, Montgomery DW, Grant OC, Fuster MM, Fu L, Dordick JS, Woods RJ, Zhang F, Linhardt RJ. 2020. Characterization of heparin and severe acute respiratory syndrome-related coronavirus 2 (SARS-CoV-2) spike glycoprotein binding interactions. Antiviral Res 181:104873. https://doi.org/10.1016/j.antiviral.2020.104873.
6. Hoffmann M, Kleine-Weber H, Schroeder S, Kruger N, Herrler T, Erichsen S, Schiergens TS, Herrler G, Wu NH, Nitsche A, Muller MA, Drosten C, Pohlmann S. 2020. SARS-CoV-2 cell entry depends on ACE2 and TMPRSS2 and is blocked by a clinically proven protease inhibitor. Cell 181:271–280.E8. https://doi.org/10.1016/j.cell.2020.02.052.
7. Clausen TM, Sandoval DR, Spliid CB, Pihl J, Perrett HR, Painter CD, Narayanan A, Majowicz SA, Kwong EM, McVicar RN, Thacker BE, Glass CA, Yang Z, Torres JL, Golden GJ, Bartels PL, Porell RN, Garretson AF, Laubach L, Feldman J, Yin X, Pu Y, Hauser BM, Caradonna TM, Kellman BP, Martino C, Gordts P, Chanda SK, Schmidt AG, Godula K, Leibel SL, Jose J, Corbett KD, Ward AB, Carlin AF, Esko JD. 2020. SARS-CoV-2 infection depends on cellular heparan sulfate and ACE2. Cell https://doi.org/10.1016/j.cell.2020.09.033.
8. Watanabe R, Sawicki SG, Taguchi F. 2007. Heparan sulfate is a binding molecule but not a receptor for CEACAM1-independent infection of murine coronavirus. Virology 366:16–22. https://doi.org/10.1016/j.virol.2007.06.034.
9. Mycroft-West CJ, Su D, Pagani I, Rudd TR, Elli S, Guimond SE, Miller G, Meneghetti MCZ, Nader HB, Li Y, Nunes QM, Procter P, Mancini N, Clementi M, Bisio A, Forsyth NR, Turnbull JE, Guerrini M, Fernig DG, Vicenzi E, Yates EA, Lima MA, Skidmore MA. 2020. Heparin inhibits cellular invasion by SARS-CoV-2: structural dependence of the interaction of the surface protein (spike) S1 receptor binding domain with heparin. bioRxiv https://www.biorxiv.org/content/10.1101/2020.04.28.066761v1.
10. Davis AE, Smallman LA. 1988. An ultrastructural study of the mucosal surface of the human inferior concha. I. Normal appearances. J Anat 161:61–71.
11. Lin B, Qing X, Liao J, Zhuo K. 2020. Role of protein glycosylation in host-pathogen interaction. Cells 9:1022. https://doi.org/10.3390/cells9041022.
12. Milho R, Frederico B, Efstathiou S, Stevenson PG. 2012. A heparan-dependent herpesvirus targets the olfactory neuroepithelium for host entry. PLoS Pathog 8:e1002986. https://doi.org/10.1371/journal.ppat.1002986.
13. Centers for Disease Control and Prevention. 2020. Interim laboratory biosafety guidelines for handling and processing specimens associated with coronavirus disease 2019 (COVID-19). Centers for Disease Control and Prevention, Atlanta, GA. https://www.cdc.gov/coronavirus/2019-ncov/lab/lab-biosafety-guidelines.html.
14. Arnold J, Ahsan F, Meezan E, Pillion DJ. 2002. Nasal administration of low molecular weight heparin. J Pharm Sci 91:1707–1714. https://doi.org/10.1002/jps.10171.
15. Bendstrup KE, Chambers CB, Jensen JI, Newhouse MT. 1999. Lung deposition and clearance of inhaled (99m)Tc-heparin in healthy volunteers. Am J Respir Crit Care Med 160:1653–1658. https://doi.org/10.1164/ajrccm.160.5.9809123.
16. Bendstrup KE, Gram J, Jensen JI. 2002. Effect of inhaled heparin on lung function and coagulation in healthy volunteers. Eur Respir J 19:606–610. https://doi.org/10.1183/09031936.02.00105202.
17. Sungnak W, Huang N, Becavin C, Berg M, Queen R, Litvinukova M, Talavera-Lopez C, Maatz H, Reichart D, Sampaziotis F, Worlock KB, Yoshida M, Barnes JL, HCA Lung Biological Network. 2020. SARS-CoV-2 entry factors are highly expressed in nasal epithelial cells together with innate immune genes. Nat Med 26:681–687. https://doi.org/10.1038/s41591-020-0868-6.
18. Wolfel R, Corman VM, Guggemos W, Seilmaier M, Zange S, Muller MA,

Niemeyer D, Jones TC, Vollmar P, Rothe C, Hoelscher M, Bleicker T, Brunink S, Schneider J, Ehmann R, Zwirglmaier K, Drosten C, Wendtner C. 2020. Virological assessment of hospitalized patients with COVID-2019. Nature 581:465–469. https://doi.org/10.1038/s41586-020-2196-x.
19. Zhou P, Yang XL, Wang XG, Hu B, Zhang L, Zhang W, Si HR, Zhu Y, Li B, Huang CL, Chen HD, Chen J, Luo Y, Guo H, Jiang RD, Liu MQ, Chen Y, Shen XR, Wang X, Zheng XS, Zhao K, Chen QJ, Deng F, Liu LL, Yan B, Zhan FX, Wang YY, Xiao GF, Shi ZL. 2020. A pneumonia outbreak associated with a new coronavirus of probable bat origin. Nature 579:270–273. https://doi.org/10.1038/s41586-020-2012-7.
20. Dull T, Zufferey R, Kelly M, Mandel RJ, Nguyen M, Trono D, Naldini L. 1998. A third-generation lentivirus vector with a conditional packaging system. J Virol 72:8463–8471. https://doi.org/10.1128/JVI.72.11.8463-8471.1998.
21. Follenzi A, Naldini L. 2002. Generation of HIV-1 derived lentiviral vectors. Methods Enzymol 346:454–465. https://doi.org/10.1016/s0076-6879(02)46071-5.
22. Ticar BF, Rohmah Z, Neri TAN, Pahila IG, Vasconcelos A, Archer-Hartmann SA, Reiter CEN, Dobruchowska JM, Choi BD, Heiss C, Azadi P, Pomin VH. 2020. Biocompatibility and structural characterization of glycosaminoglycans isolated from heads of silver-banded whiting (Sillago argentifasciata Martin & Montalban 1935). Int J Biol Macromol 151:663–676. https://doi.org/10.1016/j.ijbiomac.2020.02.160.
23. Pomin VH. 2012. Fucanomics and galactanomics: current status in drug discovery, mechanisms of action and role of the well-defined structures. Biochim Biophys Acta 1820:1971–1979. https://doi.org/10.1016/j.bbagen.2012.08.022.
24. Krishna NK, Campbell S, Vogt VM, Wills JW. 1998. Genetic determinants of Rous sarcoma virus particle size. J Virol 72:564–577. https://doi.org/10.1128/JVI.72.1.564-577.1998.
25. Vogt VM, Simon MN. 1999. Mass determination of rous sarcoma virus virions by scanning transmission electron microscopy. J Virol 73:7050–7055. https://doi.org/10.1128/JVI.73.8.7050-7055.1999.
26. Zong C, Huang R, Condac E, Chiu Y, Xiao W, Li X, Lu W, Ishihara M, Wang S, Ramiah A, Stickney M, Azadi P, Amster IJ, Moremen KW, Wang L, Sharp JS, Boons GJ. 2016. Integrated approach to identify heparan sulfate ligand requirements of Robo1. J Am Chem Soc 138:13059–13067. https://doi.org/10.1021/jacs.6b08161.
27. Li Z, Moniz H, Wang S, Ramiah A, Zhang F, Moremen KW, Linhardt RJ, Sharp JS. 2015. High structural resolution hydroxyl radical protein footprinting reveals an extended Robo1-heparin binding interface. J Biol Chem 290:10729–10740. https://doi.org/10.1074/jbc.M115.648410.
28. Seyedpour S, Khodaei B, Loghman AH, Seyedpour N, Kisomi MF, Balibegloo M, Nezamabadi SS, Gholami B, Saghazadeh A, Rezaei N. 2020. Targeted therapy strategies against SARS-CoV-2 cell entry mechanisms: a systematic review of in vitro and in vivo studies. J Cell Physiol https://doi.org/10.1002/jcp.30032.
29. Wu D, Koganti R, Lambe UP, Yadavalli T, Nandi SS, Shukla D. 2020. Vaccines and therapies in development for SARS-CoV-2 infections. J Clin Med 9:1885. https://doi.org/10.3390/jcm9061885.
30. Shi C, Wang C, Wang H, Yang C, Cai F, Zeng F, Cheng F, Liu Y, Zhou T, Deng B, Vlodavsky I, Li J, Zhang Y. 2020. The potential of low molecular weight heparin to mitigate cytokine storm in severe COVID-19 patients: a retrospective clinical study. medRxiv https://www.medrxiv.org/content/10.1101/2020.03.28.20046144v3.
31. Johansen KB. 17 December 1987, publication date. Pharmaceutical composition for the nasal administration of heparin and method for treatment of patients. International patent application WO 87/07504.
32. Weyers A, Yang B, Solakyildirim K, Yee V, Li L, Zhang F, Linhardt RJ. 2013. Isolation of bovine corneal keratan sulfate and its growth factor and morphogen binding. FEBS J 280:2285–2293. https://doi.org/10.1111/febs.12165.
33. Lin YP, Yu Y, Marcinkiewicz AL, Lederman P, Hart TM, Zhang F, Linhardt RJ. 2020. Non-anticoagulant heparin as a pre-exposure prophylaxis prevents Lyme disease infection. ACS Infect Dis 6:503–514. https://doi.org/10.1021/acsinfecdis.9b00425.
34. Cress BF, Bhaskar U, Vaidyanathan D, Williams A, Cai C, Liu X, Fu L, M-Chari V, Zhang F, Mousa SA, Dordick JS, Koffas MAG, Linhardt RJ. 2019. Heavy heparin: a stable isotope-enriched, chemoenzymatically-synthesized, poly-component drug. Angew Chem Int Ed Engl 58:5962–5966. https://doi.org/10.1002/anie.201900768.
35. Huang R, Pomin VH, Sharp JS. 2011. LC-MS^n analysis of isomeric chondroitin sulfate oligosaccharides using a chemical derivatization strategy. J Am Soc Mass Spectrom 22:1577–1587. https://doi.org/10.1007/s13361-011-0174-0.
36. Inoue Y, Nagasawa K. 1976. Selective N-desulfation of heparin with dimethyl sulfoxide containing water or methanol. Carbohydr Res 46:87–95. https://doi.org/10.1016/S0008-6215(00)83533-8.
37. Kariya Y, Kyogashima M, Suzuki K, Isomura T, Sakamoto T, Horie K, Ishihara M, Takano R, Kamei K, Hara S. 2000. Preparation of completely 6-O-desulfated heparin and its ability to enhance activity of basic fibroblast growth factor. J Biol Chem 275:25949–25958. https://doi.org/10.1074/jbc.M004140200.
38. Liang Q, Chopra P, Boons G-J, Sharp JS. 2018. Improved de novo sequencing of heparin/heparan sulfate oligosaccharides by propionylation of sites of sulfation. Carbohydr Res 465:16–21. https://doi.org/10.1016/j.carres.2018.06.002.